# Article

# Loss of p53 in Enterocytes Generates an Inflammatory Microenvironment Enabling Invasion and Lymph Node Metastasis of Carcinogen-Induced Colorectal Tumors

Sarah Schwitalla,[1] Paul K. Ziegler,[1] David Horst,[2] Valentin Becker,[3] Irina Kerle,[1] Yvonne Begus-Nahrmann,[6] André Lechel,[6] K. Lenhard Rudolph,[6] Rupert Langer,[4] Julia Slotta-Huspenina,[4] Franz G. Bader,[5] Olivia Prazeres da Costa,[7] Markus F. Neurath,[8] Alexander Meining,[3] Thomas Kirchner,[2] and Florian R. Greten[1,*]

[1]Institute of Molecular Immunology, Klinikum rechts der Isar, Technical University Munich, Trogerstrasse 9, 81675 Munich, Germany
[2]Institute of Pathology, Ludwig-Maximilians-University, 80337 Munich, Germany
[3]Second Department of Medicine
[4]Institute of Pathology
[5]Department of General Surgery
Klinikum rechts der Isar, Technical University Munich, Ismaningerstrasse 22, 81675 Munich, Germany
[6]Institute of Molecular Medicine, Max-Planck-Research Department on Stem Cell Aging, Ulm University, Albert-Einstein-Allee 11, 89075 Ulm, Germany
[7]Institute of Medical Microbiology, Immunology and Hygiene, Technical University Munich, Trogerstrasse 30, 81675 Munich, Germany
[8]Medical Clinic 1, Friedrich-Alexander-Universität Erlangen-Nürnberg, Ulmenweg 18, 91054 Erlangen, Germany
*Correspondence: florian.greten@lrz.tum.de
http://dx.doi.org/10.1016/j.ccr.2012.11.014

## SUMMARY

Loss of p53 is considered to allow progression of colorectal tumors from the adenoma to the carcinoma stage. Using mice with an intestinal epithelial cell (IEC)-specific p53 deletion, we demonstrate that loss of p53 alone is insufficient to initiate intestinal tumorigenesis but markedly enhances carcinogen-induced tumor incidence and leads to invasive cancer and lymph node metastasis. Whereas p53 controls DNA damage and IEC survival during the initiation stage, loss of p53 during tumor progression is associated with increased intestinal permeability, causing formation of an NF-κB-dependent inflammatory microenvironment and the induction of epithelial-mesenchymal transition. Thus, we propose a p53-controlled tumor-suppressive function that is independent of its well-established role in cell-cycle regulation, apoptosis, and senescence.

## INTRODUCTION

The development of invasive cancer is a multistep process involving mutations in tumor-suppressor genes and proto-oncogenes that are successively acquired over several decades (Hahn and Weinberg, 2002). Such accumulation of genetic alterations correlating with tumors ranging from benign adenomas to invasive cancer was first proposed for colorectal carcinogenesis (Vogelstein et al., 1988). Mutations in *APC* or *CTNNB1* are found in the majority of colorectal tumors, and thus activation of the Wnt pathway has been suggested to serve

as a gatekeeper of colorectal tumor development (Fodde et al., 2001). Other key proteins that are proposed to be affected at different stages in this adenoma-to-carcinoma progression model are K-RAS, SMAD4, DCC, and p53 (Fearon and Vogelstein, 1990). Among these, p53 is considered one of the most important tumor suppressors for not only colorectal carcinogenesis but also nearly all malignancies. Upon DNA damage or oncogenic stress, wild-type p53 guards the genome and maintains genomic stability by transcriptional regulating genes involved in apoptosis, cell-cycle arrest, senescence, or DNA repair (Riley et al., 2008). Therefore, loss of this essential tumor

### Significance

We demonstrate that p53 in intestinal epithelial cells confers two different tumor-suppressive mechanisms during early- and late-stage carcinogenesis. These results provide functional evidence for an essential role of p53 during colorectal tumor invasion and metastasis and unravel a function of this tumor suppressor in the creation of an inflammatory microenvironment. Furthermore, we establish a valuable mouse model of colorectal carcinogenesis that will be useful for translational studies such as the preclinical assessment of potential therapeutic regimens or the longitudinal evaluation of in vivo imaging approaches.

suppressor provides a tumor cell with substantial growth advantages. In the colorectal tumor progression model, loss of p53 tumor suppressor function has been suggested to occur at the transition stage from late adenomas to invasive carcinoma (Vogelstein et al., 1988). Although recent genetic studies have confirmed that *TP53* is one of the most commonly mutated genes in human colorectal cancer (Wood et al., 2007), functional evidence supporting an essential role for p53 to specifically suppress colorectal tumor invasion is, however, still lacking.

Apart from the successive acquisition of mutations that provide tumor cells with a cell-autonomous growth advantage, an inflammatory tumor microenvironment represents another prerequisite for all stages of tumor development (Grivennikov et al., 2010) and has recently been included in the revised hallmarks of cancer (Hanahan and Weinberg, 2011). Activation of certain oncogenes initiates an intrinsic inflammatory response that is characterized by the expression of tumor-promoting chemokines and cytokines as well as the recruitment of innate immune cells (Mantovani et al., 2008). This leads to the activation of fibroblasts, matrix remodeling, angiogenesis, and the release of soluble mediators that promote survival of initiated malignant cells in a paracrine manner (Grivennikov et al., 2010). Furthermore, the existence of an inflammatory microenvironment is considered to provide the basis for invasion and metastasis (Joyce and Pollard, 2009). The two transcription factors NF-κB and STAT3 comprise two central signaling pathways in the inflammatory tumor microenvironment because they control various protumorigenic processes such as growth, proliferation, survival, angiogenesis, and invasion (Bollrath and Greten, 2009). Moreover, in initiated neoplastic cells, they regulate the production of chemokines that attract cytokine-secreting inflammatory cells, which lead to further NF-κB and STAT3 activation in tumor cells and therefore participate in a positive feedforward loop that sustains tumor-associated inflammation (Grivennikov et al., 2010).

Here, we aimed to examine the intestinal epithelial cell (IEC)-specific tumor-suppressive function of p53 and the potential involvement of NF-κB during tumor progression.

## RESULTS

### Loss of *Tp53* in IECs Is Not Sufficient to Initiate Intestinal Neoplasia

To specifically examine the functional role of p53 in IEC homeostasis as well as during intestinal tumor development, we crossed *villin*-Cre mice (Madison et al., 2002) to *Tp53*[F/F] mice (Jonkers et al., 2001). The resulting mice lacking exons 2–10 of *Tp53* in their IECs, termed *Tp53*[ΔIEC], developed normally and were healthy and fertile. IEC-specific loss of *Tp53* did not disturb the frequency of intestinal stem cells or intestinal differentiation (see Figures S1A–S1G available online), and importantly had no effect on baseline proliferation or apoptosis of unchallenged mice (Figures S1H and S1I). Consequently, loss of p53 did not provide a growth advantage in ex-vivo-induced crypt organoid formation (Figure S1J) and did not lead to spontaneous intestinal tumor formation when mice were monitored up to 14 months (n = 20). In order to test the effect of IEC-restricted p53 loss in a Wnt-driven model of intestinal tumorigenesis, we challenged *Tp53*[ΔIEC] mice repetitively with the carcinogen azoxymethane

(AOM). AOM is known to induce mutations in exon 3 of *Ctnnb*, which causes constitutive activation of the Wnt pathway by stabilizing β-catenin (Greten et al., 2004). When mice were analyzed 16 weeks after the first AOM administration, colonic tumor incidence was markedly increased in *Tp53*[ΔIEC] mice compared to *Tp53*-proficient littermate controls (Figures 1A, 1E, and 1F). However, loss of p53 affected tumor incidence but not tumor size (Figure 1B). Accordingly, proliferation index and apoptotic index were not significantly different in tumors between these genotypes (Figures 1C and 1D). Tumors of both genotypes had a classical tubular morphology, whereas some *Tp53*-deficient tumors were less differentiated (Figures 1G, 1H, and 1J). Whereas tumors in wild-type animals were exclusively located in the distal colon, 18% of *Tp53*[ΔIEC] mice also developed small intestinal tumors in addition to the colonic tumors. Most importantly, at 16 weeks in all *Tp53*[ΔIEC] mice, more than 50% of the colonic tumors had invaded into the submucosa (Figures 1I and 1J). In contrast, invasive tumors were never detected in control animals at this or even later time points. When we monitored AOM-injected *Tp53*[ΔIEC] mice for more than 20 weeks, invasion had progressed through all intestinal layers and tumor expansion could even be observed along the outer intestinal wall (Figure 1J). Moreover, 7 out 23 *Tp53*[ΔIEC] mice (30%) had developed lymph node metastases expressing nuclear β-catenin by 24 weeks (Figures 1K and 1L), yet no metastases could be detected in other organs such as lung or liver.

### Elimination of Early AOM-Initiated IECs Is Impaired in *Tp53*[ΔIEC] Mice

AOM is considered to induce a p53-dependent apoptotic wave in IECs within the first hours after administration (Toft et al., 1999). Thus, we reasoned that loss of p53 in IECs may suppress this initial apoptotic response, thereby preventing loss of initiated epithelia that would subsequently increase tumor incidence (Greten et al., 2004; Qiu et al., 2009). Indeed, IEC-restricted p53 deficiency prevented the initial AOM-induced epithelial apoptosis (Figures 2A–2C) and led to a substantially increased number of phospho-H2A.X-positive colonic IECs (Figures 2D and 2E). This was associated with the decreased expression of genes encoding the proapoptotic proteins Bax, Puma, Noxa, and Trail as well as Mgmt (Figure 2F), which is mainly responsible for the repair of $O^6$-methylguanine-containing DNA adducts, suggesting that p53 controls both apoptosis and DNA repair in colonic IECs after exposure to AOM. Furthermore, the lack of apoptosis and thus the increased survival of DNA-damaged IECs supported the notion that the diminished elimination of mutagenized IECs accounts for the elevated tumor incidence observed in *Tp53*[ΔIEC] mice. To confirm this, we crossed *Tp53*[F/F] mice to *villin-cre*ER[T2] mice (el Marjou et al., 2004) and compared tumor incidence as well as extent of invasion in *villin-cre*ER[T2];*Tp53*[F/F] receiving tamoxifen before or after challenge with AOM (Figure 2G). As hypothesized, deletion of *Tp53* before AOM administration led to a significantly higher tumor incidence (Figures 2H and 2I) but did not affect tumor size, thus mimicking the situation observed in *Tp53*[ΔIEC] mice with constitutive Cre-recombinase expression. Importantly, however, the extent of invasion was independent of the timing of *Tp53* loss (Figure 2J), indicating that in AOM-induced
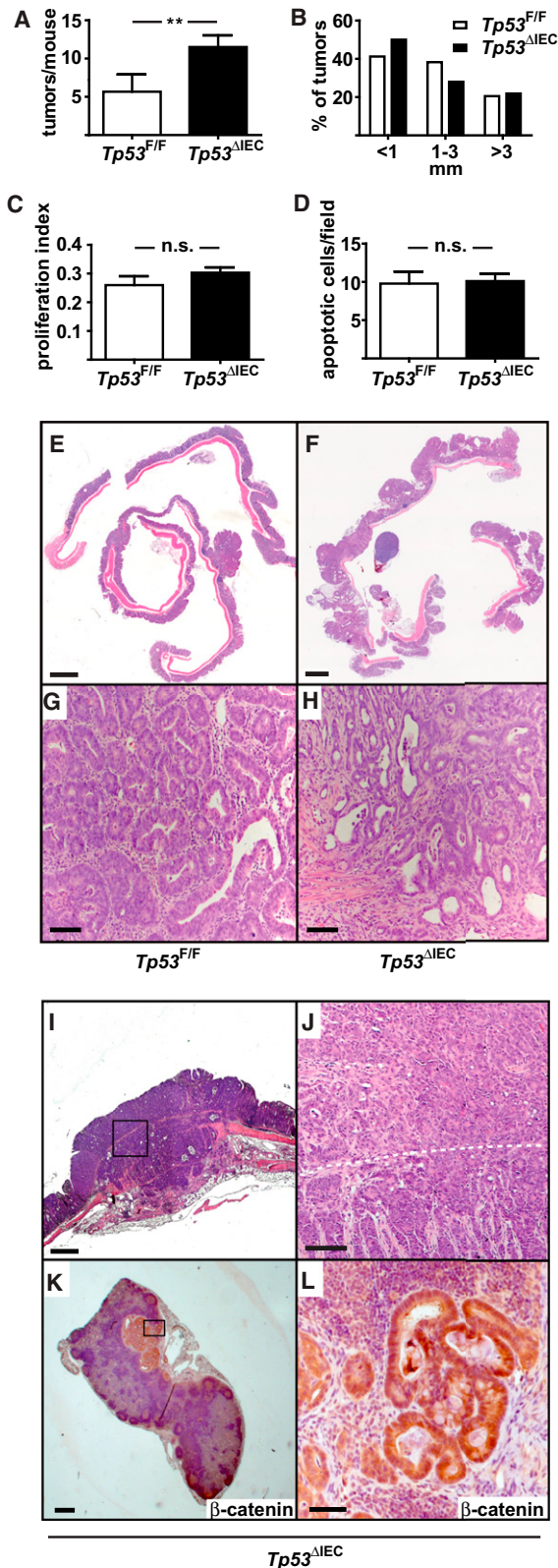
tumorigenesis, p53 controls tumor incidence and invasion via two distinct mechanisms.

### Invasion in *Tp53*-Deficient AOM-Initiated Tumors Is Associated with Upregulation of Genes Involved in Inflammation and Epithelial-Mesenchymal Transition

Although p53 is involved in the maintenance of chromosomal stability (Levine and Oren, 2009), invasive tumors in AOM-induced *Tp53*$^{\Delta IEC}$ mice had only a few chromosomal aberrations and thus were not associated with chromosomal instability (Figure S2). To further elucidate the mechanisms that allowed invasion of AOM-induced tumors in *Tp53*$^{\Delta IEC}$ mice, we isolated RNA from wild-type and *Tp53*-deficient tumors at 16 weeks and performed a microarray analysis. A total of 370 genes was significantly differentially expressed, of which 223 were upregulated and 147 were downregulated by at least 2-fold in *Tp53*-deficient tumors compared with wild-type adenomas. Interestingly, the largest group of upregulated genes was associated with chemotaxis, prostaglandin synthesis, and inflammation (Figure 3A) including but not restricted to *Cxcl1*, *Cxcl2*, *Cxcl10*, *Ccl2*, *Ccl11*, *Ccl21*, *Ptgs2*, *Lifr*, and *Il11*, which was confirmed by real-time PCR (Figure 3B). The second-largest set of upregulated genes in *Tp53*-deficient tumors was associated with cell adhesion and morphogenesis and included genes coding for Twist, versican, tenascin C, and fibronectin 1, well-known regulators of metastasis and epithelial-mesenchymal transition (EMT), a key process for invasion and metastasis of solid tumors (Polyak and Weinberg, 2009). In accordance with the occurrence of EMT, E-cadherin mRNA level was downregulated (Figure 3C). Another prerequisite for tumor invasion is the activation and release of stromal cell-derived proteases such as cathepsins and matrix metalloproteases (Joyce and Pollard, 2009). Indeed, expression of *Ctsl1*, *Mmp2*, *Mmp3*, *Mmp10*, and *Mmp13* was elevated in tumors of *Tp53*$^{\Delta IEC}$ mice, whereas *Ctsb*, *Ctss*, and *Mmp9* levels were comparable to wild-type tumors (Figure 3D).

### Enrichment of NF-κB Target Genes in p53-Deficient Tumors

Because several of the genes we found upregulated in p53-deficient tumors, including *Cxcl1*, *Cxcl10*, *Ctsl1*, *Twist*, and

(B) Histogram showing size distribution of tumors.
(C) BrdU proliferation index of epithelial tumor cells in AOM-induced tumors in *Tp53*$^{F/F}$ and *Tp53*$^{\Delta IEC}$ mice. Data are mean ± SE; n ≥ 10 tumors of each genotype. n.s., not significant.
(D) Number of cleaved caspase-3-positive epithelial tumor cells in AOM-induced tumors in *Tp53*$^{F/F}$ and *Tp53*$^{\Delta IEC}$ mice. Data are mean ± SE; n ≥ 10 tumors of each genotype.
(E–H) Hematoxylin and eosin (H&E)-stained sections of colons from mice at 16 weeks after the first AOM injection, showing representative tumor morphology in *Tp53*$^{F/F}$ (E and G) and *Tp53*$^{\Delta IEC}$ mice (F and H). Scale bars represent 1,000 μm (E and F) and 50 μm (G and H).
(I and J) H&E-stained section showing representative invasive colon carcinoma in AOM-challenged *Tp53*$^{\Delta IEC}$ mice. A larger magnification of the boxed area in (I) is depicted in (J). Scale bars represent 1,000 μm (I) and 100 μm (J).
(K and L) Immunohistochemical analysis of β-catenin in a lymph node metastasis occurring in AOM-challenged *Tp53*$^{\Delta IEC}$ mice. A larger magnification of the boxed area in (K) is depicted in (L). Scale bars represent 500 μm (K) and 50 μm (L).
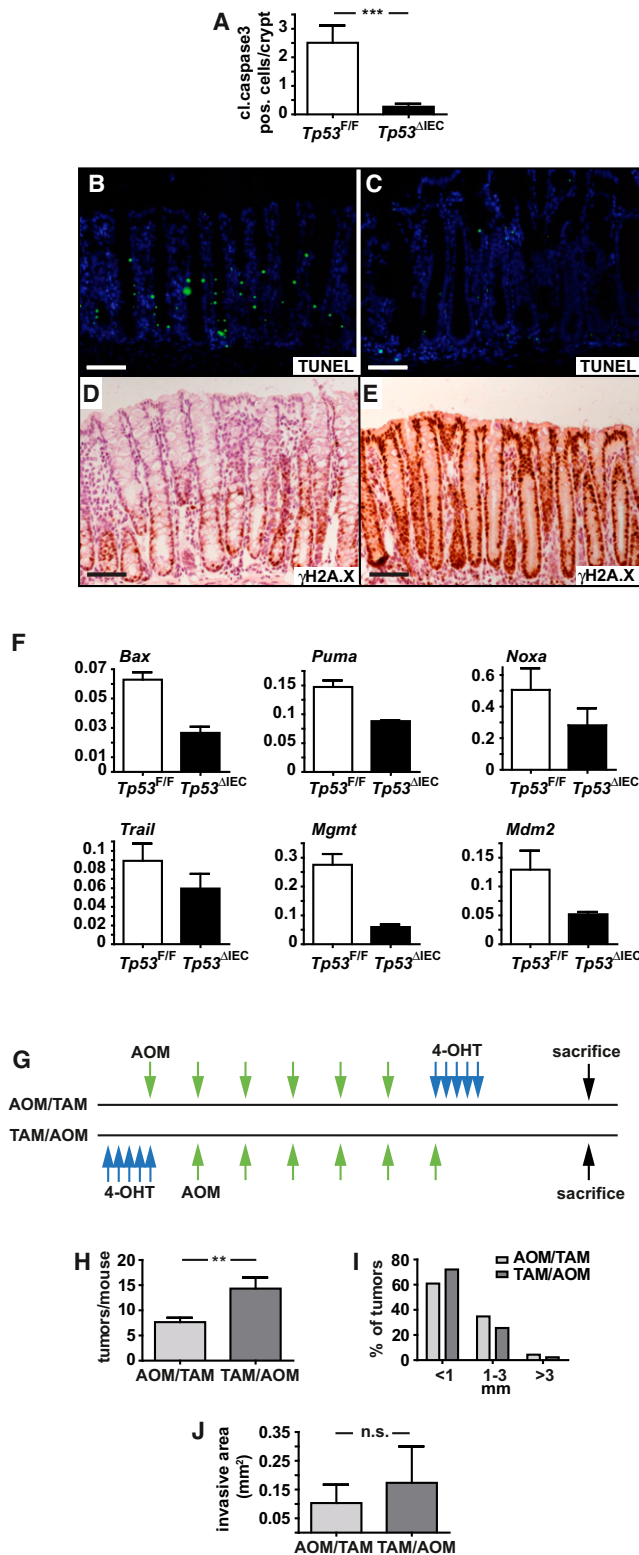See also Figure S1.

**Figure 1. Increased Tumor Incidence and Invasion in *Tp53*$^{\Delta IEC}$ Mice after AOM Treatment**
(A) Tumor incidence in *Tp53*$^{F/F}$ and *Tp53*$^{\Delta IEC}$ mice 16 weeks after the first of six weekly AOM injections. Data are mean ± SE; n ≥ 7; **p < 0.001 by t test.

*Tnc*, are well-established NF-κB target genes and are overexpressed in cells at the invasion front compared to cells in the center of the same tumor (Horst et al., 2009), we performed cross-species gene set enrichment analysis (GSEA) to compare our data set with genes that are differentially expressed in human colon cancer cells along the invasion front. Indeed, GSEA showed a strong correlation with and a high enrichment of this particular set of NF-κB target genes in p53-deficient cancers, but not in noninvasive wild-type adenomas (Figure 4A), that were paralleled by marked phosphorylation of IκBα and RelA/p65 (Figure 4B). Phosphorylated RelA/p65 was detectable both in tumor epithelia as well as in the surrounding stromal cells (Figure 4C). Furthermore, CXCL1, whose human gene is one of the most upregulated in human invading tumor cells (Horst et al., 2009), was also strongly expressed in murine tumor epithelia along the invasion front (Figure 4D). CXCL1, CXCL2, and CCL2 are potent chemoattractants of myeloid cells, and have therefore been suggested to play an important role during tumor development (Murdoch et al., 2008). Indeed, F4/80[+] and Gr1^{+} myeloid cells were localized particularly around the basal membrane along the invasion front of tumors (Figures 4E and 4F). In contrast, these cells were less abundant and more evenly distributed in noninvasive wild-type adenomas (Figure S3). Furthermore, CD3^{+} T cells and B220^{+} B cells were found only infrequently at the invasion front (data not shown). Marked upregulation of Twist was confirmed by immunoblot analysis in p53-deficient cancers (Figure 4G) and could be detected in spindle-like-shaped adenomatous cells (Figure 4H). In agreement with EMT induction, expression of vimentin could be observed in p53-deficient E-cadherin^{+} epithelial cells (Figure 4I) but not in p53-proficient adenomatous epithelia (data not shown). Collectively, these data indicate that during AOM-induced carcinogenesis, IEC-specific loss of *Tp53* leads to a myeloid cell-dominated inflammatory microenvironment associated with NF-κB activation facilitating EMT and invasion.

To test whether NF-κB activation was associated with loss of p53 function and myeloid cell recruitment in human colon cancer, we examined surgically resected invasive colon cancer specimens from 59 patients. Immunohistochemical analysis showed a positive correlation between phosphorylated, activated p65 and p53 overexpression, which serves as a marker for the presence of p53 mutations (Figures 4J–4N). Importantly,

**Figure 2. Impaired Apoptosis and Increased DNA Damage after AOM Application**

(A) Number of cleaved caspase-3-positive colonic IECs 8 hr after AOM injection in *Tp53*[F/F] and *Tp53*[ΔIEC] mice. Data are mean ± SE of 50 well-oriented crypts in two animals of each genotype; ***p < 0.0001 by t test.

(B–E) Representative TUNEL staining (B and C) and immunohistochemical analysis of γH2A.X (D and E) in colons of *Tp53*[F/F] and *Tp53*[ΔIEC] mice 8 hr after AOM injection. Scale bars represent 50 μm.

(F) Relative mRNA levels in colonic IECs of *Tp53*[F/F] and *Tp53*[ΔIEC] mice 8 hr after AOM injection. mRNA levels represent the mean ± SE of a minimum of two animals of each genotype.

(G) Schematic representation of the order of AOM and tamoxifen (TAM) application in inducible *villin-cre*ER[T2];*Tp53*[F/F] mice. 4-OHT, 4-hydroxytamoxifen.

(H) Tumor incidence in *villin-cre*ER[T2];*Tp53*[F/F] mice 16 weeks after the first of six weekly AOM injections that had received AOM before (AOM/TAM) or after tamoxifen (TAM/AOM). Data are mean ± SE; n ≥ 3; **p < 0.001 by t test. Note that tumor incidence in AOM/TAM-treated *villin-cre*ER[T2];*Tp53*[F/F] mice was comparable to equally treated wild-type mice (data not shown).

(I) Histogram showing size distribution of tumors.

(J) Average invasive area in colonic tumors of *villin-cre*ER[T2];*Tp53*[F/F] mice that had received AOM before (AOM/TAM) or after tamoxifen (TAM/AOM). Data are mean ± SE; n ≥ 3. n.s., not significant.
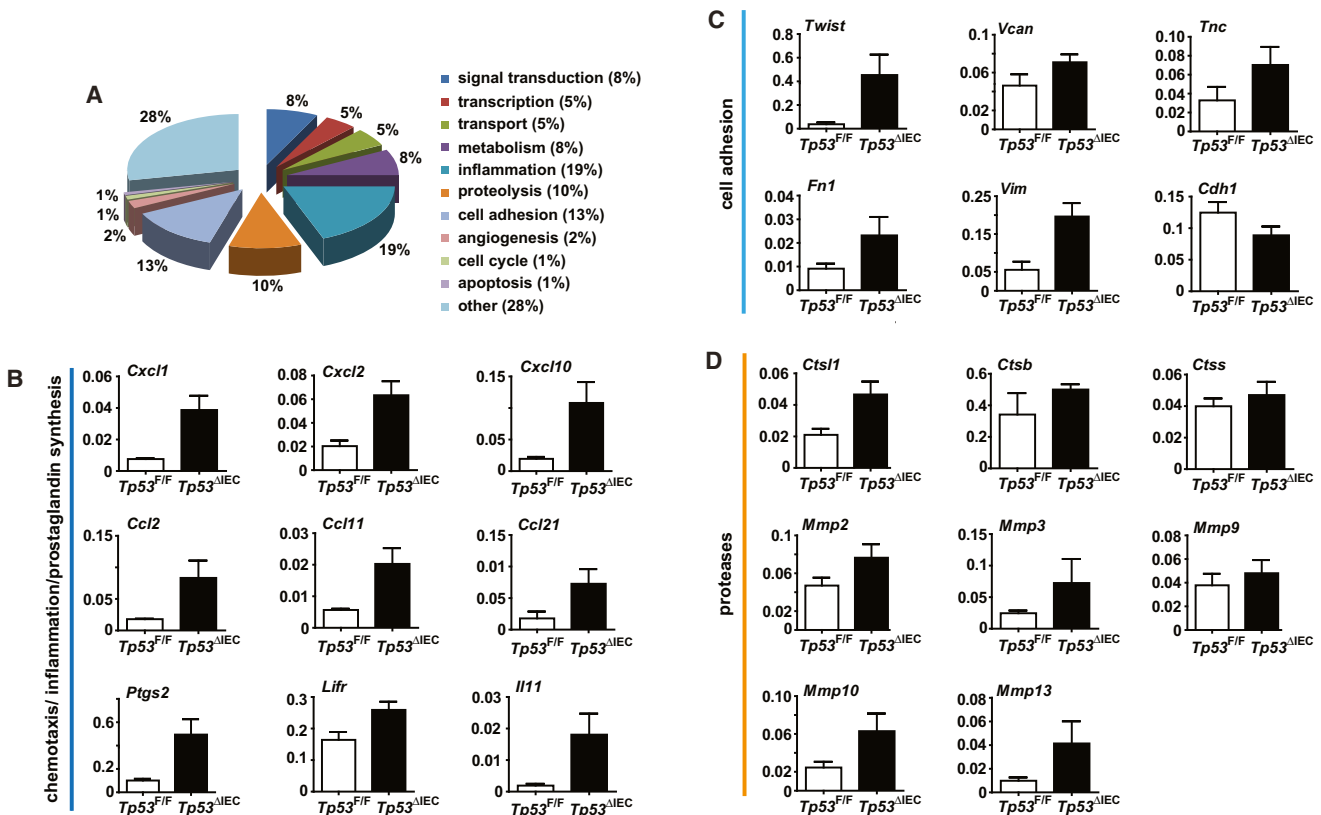
**Figure 3. Development of an Inflammatory Microenvironment and EMT in p53-Deficient Invasive Carcinoma**

(A) Graph displays the percentage of genes that were at least 2-fold upregulated in invasive cancers from $Tp53^{\Delta IEC}$ mice compared to noninvasive adenomas from $Tp53^{F/F}$ mice 16 weeks after the first AOM administration. Genes were sorted by their membership in KEGG pathways. Note that the group "inflammation" contains genes involved in chemotaxis, inflammation, and prostaglandin synthesis.

(B–D) Relative expression levels of indicated mRNAs isolated from AOM-induced tumor tissues of $Tp53^{F/F}$ and $Tp53^{\Delta IEC}$ mice and analyzed by real-time PCR. Data are mean ± SE; n ≥ 3.

See also Figure S2.

tumors expressing activated p65 and overexpressing p53 were also characterized by a significant upregulation of the macrophage-specific surface marker CD68 (Figures 4P–4R). In contrast, expression of the neutrophil-specific marker myeloperoxidase was indifferent among various groups (data not shown). Moreover, activation of NF-κB also correlated with the occurrence of lymph node metastases in this patient cohort (Figure 4O). Thus, our findings in cancers from AOM-initiated $Tp53^{\Delta IEC}$ mice closely recapitulate the situation in human colon cancer.

### Intestinal Barrier Function Is Impaired in AOM-Challenged $Tp53^{\Delta IEC}$ Mice

To examine whether loss of p53 in IECs led to elevated NF-κB activation in a cell-autonomous manner, we injected $Tp53^{\Delta IEC}$ mice with lipopolysaccharide (LPS), a potent inducer of NF-κB in IECs (Egan et al., 2004). However, neither basal nor LPS-induced NF-κB DNA binding was elevated in the mucosa of $Tp53^{\Delta IEC}$ mice (Figures S4A–S4C). Moreover, expression of well-established NF-κB target genes in p53-deficient IECs was comparable to littermate controls in unchallenged mice as well as in response to LPS (Figure S4D). Furthermore, we did not

detect increased interaction of p300/CBP and NF-κB or elevated levels of *Glut3*, which were both shown to be responsible for enhanced NF-κB activity in p53-deficient cells (data not shown) (Kawauchi et al., 2008; Webster and Perkins, 1999). Collectively, these results suggested a potential cell-nonautonomous regulation of NF-κB in AOM-initiated $Tp53^{\Delta IEC}$ mice. Increased tight-junction permeability and decreased epithelial barrier function have been shown to associate with human and carcinogen-induced rodent colon carcinogenesis (Soler et al., 1999). Therefore, we examined whether loss of IEC p53 affected epithelial barrier function. Although we could not detect significant differences in unchallenged mice (data not shown), LPS plasma levels in AOM-initiated tumor-bearing $Tp53^{\Delta IEC}$ mice were about 2.5-fold higher than in control animals (Figure 5A). In line with defective tight-junction permeability in AOM-challenged animals, fluorescence in situ hybridization (FISH) revealed enhanced translocation of intestinal bacteria into tumors (Figures 5B and 5C). In p53-deficient cancers, occludin level was reduced and showed a more cytoplasmic localization compared to wild-type tumors (Figures 5D and 5E). Furthermore, expression of genes coding for several tight-junction components was affected in p53-deficient cancers (Figure 5F). In
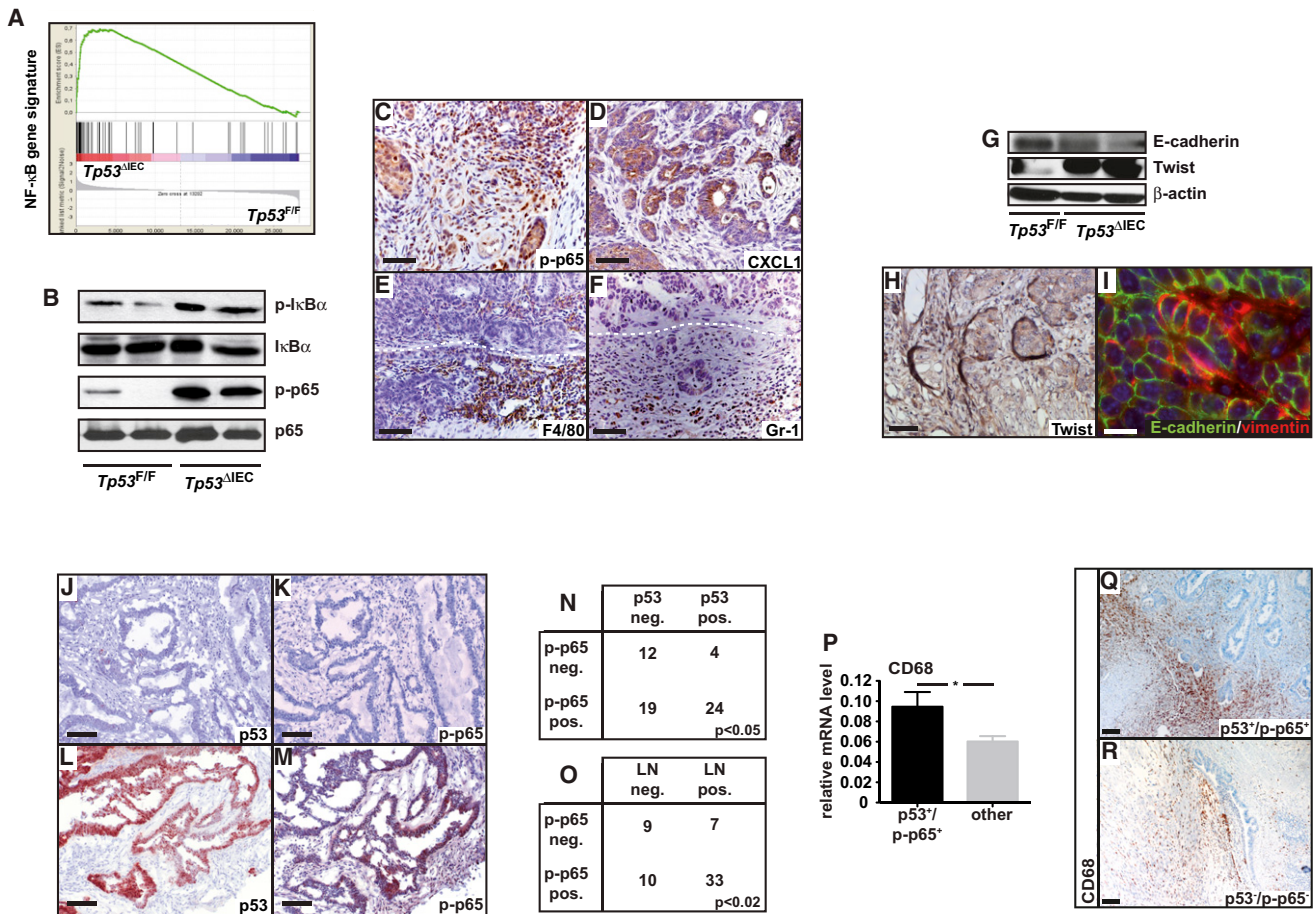
**Figure 4. Activation of NF-κB Is Associated with Cxcl1 and Twist Upregulation in p53-Deficient Invasive Carcinoma**
(A) GSEA comparing all differentially regulated genes from AOM-induced invasive cancers in $Tp53^{\Delta IEC}$ mice with a data set of NF-κB target genes obtained from microdissected invading human tumor epithelia (Horst et al., 2009). Normalized enrichment score: 1.46; p < 0.0001.
(B) Immunoblot analysis for the indicated proteins in lysates from invasive cancers from $Tp53^{\Delta IEC}$ mice and noninvasive adenomas from $Tp53^{F/F}$ mice 16 weeks after the first AOM administration.
(C–F) Immunohistochemical analysis of activated p-p65 (C), CXCL1 (D), F4/80 (E), and Gr-1 (F) in invasive cancers of AOM-challenged $Tp53^{\Delta IEC}$ mice. Dashed white lines mark the basal membrane. Scale bars represent 50 μm.
(G) Immunoblot analysis for the indicated proteins in lysates from invasive cancers from $Tp53^{\Delta IEC}$ mice and noninvasive adenomas from $Tp53^{F/F}$ mice 16 weeks after the first AOM administration.
(H) Immunohistochemical analysis of Twist in invasive cancers of AOM-challenged $Tp53^{\Delta IEC}$ mice. The scale bar represents 50 μm.
(I) Colocalization of E-cadherin (green) and vimentin (red) in invasive cancer epithelial cells of AOM-challenged $Tp53^{\Delta IEC}$ mice, indicating EMT; nuclei are stained using 4′,6-diamidino-2-phenylindole (blue). The scale bar represents 200 μm.
(J–M) Representative immunohistochemical analysis of p53 (J and L) and p-p65 (K and M) in human colon cancer samples. Scale bars represent 100 μm.
(N) Correlation of p53 staining and p-p65 staining (n = 59; $\chi^2$ test, p < 0.05).
(O) Correlation of p-p65 staining and the presence of lymph node (LN) metastases (n = 59; $\chi^2$ test, p < 0.02).
(P) Relative CD68 mRNA level in human colon cancer patients who were characterized by expression of both p53 and p-p65 (p53$^+$/p-p65$^+$; n = 23) or not (other; n = 30). Data are mean ± SE; *p < 0.05 by t test.
(Q and R) Representative immunohistochemical staining of CD68 in human colon cancer patients who were characterized by expression of both p53 and phospho-p65 (Q) or the absence of p53 and phospho-p65 (R). Scale bars represent 100 μm.
See also Figure S3.

particular, elevated levels of claudin 1 and Muc 1 as well as decreased levels of claudin 2 and JAM-A have also been associated with human colorectal cancer (Jang et al., 2002; Wang et al., 2011). To examine whether this barrier defect preceded invasive growth and could therefore be responsible for the creation of the inflammatory microenvironment in p53-deficient tumors, we orally gavaged mice with FITC-labeled dextran 4 weeks after

the last AOM injection, a time point long before invasive tumors are detectable. Even at this early stage, $Tp53^{\Delta IEC}$ mice were characterized by markedly elevated intestinal permeability and plasma LPS levels (Figure 5G and data not shown), which coincided with enhanced NF-κB activation in the mucosa of $Tp53^{\Delta IEC}$ mice (Figures 5H–5J), suggesting that differences in NF-κB signaling were caused by the defective epithelial barrier function
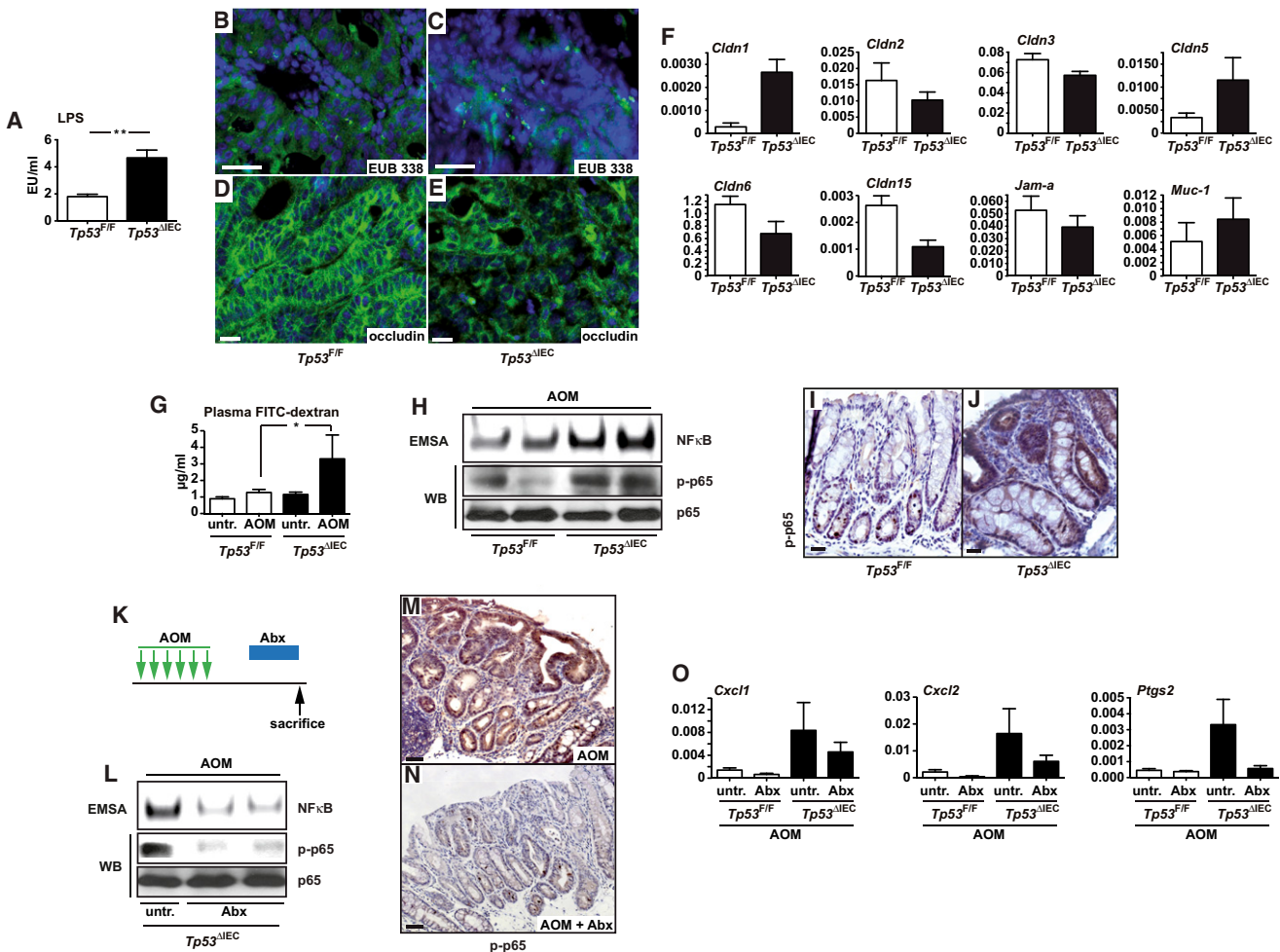
**Figure 5. Intestinal Barrier Defect in AOM-Challenged Tp53^ΔIEC Mice**

(A) Endotoxin levels in plasma collected from portal veins of $Tp53^{F/F}$ and $Tp53^{\Delta IEC}$ mice with AOM-induced tumors. Data are mean ± SE; n ≥ 3; **p < 0.001 by t test. EU, endotoxin unit.

(B and C) FISH using a FITC-labeled universal eubacteria probe (EUB 338). Scale bars represent 20 μm.

(D and E) Immunofluorescent analysis of occludin in noninvasive adenomas from $Tp53^{F/F}$ mice (D) and invasive cancers from $Tp53^{\Delta IEC}$ mice (E) 16 weeks after the first AOM administration. Scale bars represent 20 μm.

(F) Relative levels of mRNAs isolated from AOM-induced tumor tissues of $Tp53^{F/F}$ and $Tp53^{\Delta IEC}$ mice and analyzed by real-time PCR. Data are mean ± SE; n ≥ 3.

(G) FITC-dextran plasma levels 4 hr after oral gavage in unchallenged or AOM-injected $Tp53^{F/F}$ and $Tp53^{\Delta IEC}$ mice 4 weeks after the last AOM challenge. Data are mean ± SE; n = 8; *p < 0.05 by t test.

(H) Electrophoretic mobility shift assay (EMSA) and immunoblot analysis (WB) for the indicated proteins in lysates of colonic mucosa from $Tp53^{\Delta IEC}$ and $Tp53^{F/F}$ mice 4 weeks after the last AOM challenge.

(I and J) Immunohistochemical analysis of p-p65 in colonic mucosa of $Tp53^{\Delta IEC}$ and $Tp53^{F/F}$ mice 4 weeks after the last AOM challenge. Scale bars represent 20 μm.

(K) Schematic representation of the AOM and antibiotic administration. Two weeks after the completion of six weekly AOM injections, animals received a combination of vancomycin, metronidazole, ampicillin, and neomycin (Abx) in their drinking water for an additional 2 weeks prior to sacrifice.

(L) EMSA and immunoblot analysis for the indicated proteins in lysates of colonic mucosa from untreated (untr.) or antibiotic-treated (Abx) $Tp53^{\Delta IEC}$ mice 4 weeks after the last AOM challenge.

(M and N) Immunohistochemical analysis of p-p65 in colonic mucosa of untreated (M) or antibiotic-treated (N) $Tp53^{\Delta IEC}$ mice 4 weeks after the last AOM challenge. Scale bars represent 50 μm.

(O) Relative expression levels of mRNAs isolated from colonic mucosa of untreated or antibiotic-treated $Tp53^{F/F}$ and $Tp53^{\Delta IEC}$ mice 4 weeks after the last AOM challenge and analyzed by real-time PCR. Data are mean ± SE; n = 6.

See also Figure S4.

and translocation of bacteria as well as by bacterial products such as LPS. To confirm this hypothesis, we depleted the intestinal microflora by treating AOM-initiated mice with a combination of vancomycin, metronidazole, ampicillin, and neomycin for 2 weeks (Figure 5K). Successful depletion was confirmed by plating stool samples on microbiological plates. Indeed, antibiotic treatment nearly completely abolished NF-κB activation in carcinogen-challenged $Tp53^{\Delta IEC}$ mice (Figures 5L–5N) and
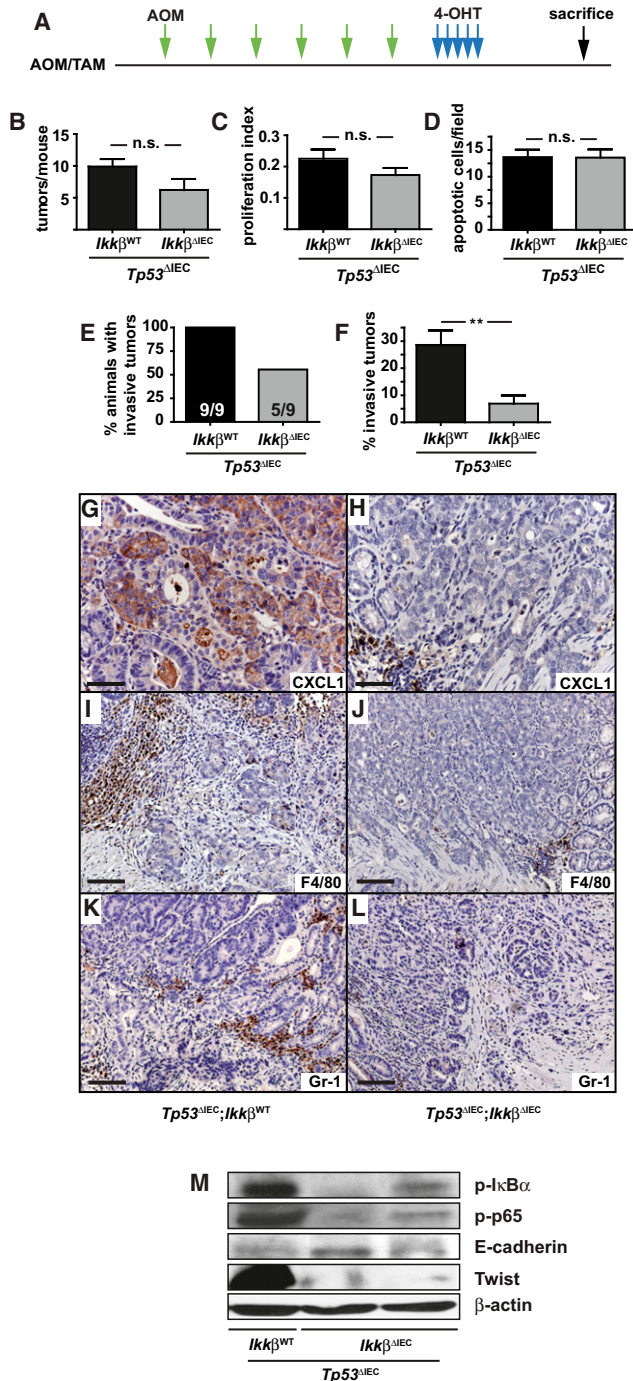
resulted in markedly decreased expression of *Cxcl1*, *Cxcl2*, and *Ptgs2* (Figure 5O). Collectively, these results suggest that in AOM-initiated IECs, loss of p53 alters the composition of tight junctions, causing an impaired barrier function and subsequently elevated circulating plasma LPS levels, which culminates in NF-κB activation and chemokine upregulation.

## Loss of IKKβ-Dependent NF-κB Activation in IECs or Myeloid Cells Reduces Invasion and Metastasis

To confirm that NF-κB signaling functionally contributes to colon cancer progression, we examined IEC- or myeloid cell-restricted loss of IKKβ in $Tp53^{\Delta IEC}$ mice. In order to specifically address IEC-specific IKKβ/NF-κB activation during the invasion stage rather than the carcinogen-induced initiation stage, we crossed $Ikk\beta^{F/F}$ mice to *villin-cre*ER$^{T2}$;$Tp53^{F/F}$ mice. Simultaneous deletion of $Ikk\beta$ and $Tp53$ in IECs was achieved by oral tamoxifen application after completion of AOM injections (Figure 6A), to exclude potential interference of AOM-triggered apoptosis and DNA-damage repair by loss of NF-κB activation in epithelial cells. Whereas IEC-restricted absence of $Ikk\beta$ did not affect tumor incidence, proliferation, or apoptosis (Figures 6B–6D), it markedly reduced the occurrence of invasive tumors. Only five out of nine $Ikk\beta^{\Delta IEC}$;$Tp53^{\Delta IEC}$ mice developed invasive lesions at all, and in these animals only 10% of tumors had invaded into the submucosa, in contrast to $Ikk\beta$ wild-type-expressing $Tp53^{\Delta IEC}$ mice, in which about 30% of tumors progressed in all animals analyzed (Figures 6E and 6F). In agreement with NF-κB's suggested role in this model and a marked decrease in the phosphorylation of IκBα and p65, CXCL1 expression (Figures 6G and 6H), accumulation of F4/80$^+$ and Gr1$^+$ myeloid cells (Figures 6I–6L), as well as Twist expression (Figure 6M) were reduced in $Ikk\beta^{\Delta IEC}$;$Tp53^{\Delta IEC}$ mice, whereas E-cadherin expression was conversely elevated (Figure 6M). These data supported the notion that NF-κB in IECs is indeed required for induction of EMT and myeloid cell recruitment.

To examine the contribution of myeloid cell-dependent NF-κB signaling to invasion and metastasis of p53-deficient carcinomas, we used *LysM*-Cre;$Ikk\beta^{F/F}$ ($Ikk\beta^{\Delta mye}$) mice. We could not directly crossbreed $Tp53^{\Delta IEC}$ to $Ikk\beta^{\Delta mye}$ mice because this would have resulted in simultaneous deletion of p53 and IKKβ in both IECs and myeloid cells. Therefore, we reconstituted lethally irradiated $Tp53^{\Delta IEC}$ mice with bone marrow from $Ikk\beta^{F/F}$ or $Ikk\beta^{\Delta mye}$ animals before the AOM challenge and monitored tumor progression (Figure 7A). Transplantation of $Ikk\beta^{\Delta mye}$ bone marrow did not affect tumor incidence or the overall frequency of invasive carcinomas in $Tp53^{\Delta IEC}$ mice (Figures 7B and 7C). However, specifically along the invasion front, which is the location where most of the macrophages and neutrophil

## Figure 6. Loss of $Ikk\beta$ in IECs Reduces Invasion in $Tp53^{\Delta IEC}$ Mice

(A) Schematic representation of the order of AOM and TAM application in inducible *villin-cre*ER$^{T2}$/$Tp53^{F/F}$ mice and *villin-cre*ER$^{T2}$/$Tp53^{F/F}$/$Ikk\beta^{F/F}$.

(B) Tumor incidence in $Tp53^{\Delta IEC}$;$Ikk\beta^{WT}$ (black bars) and $Tp53^{\Delta IEC}$;$Ikk\beta^{\Delta IEC}$ (gray bars) mice 18 weeks after tamoxifen administration. Data are mean ± SE; n = 9 animals/genotype. n.s., not significant.

(C) BrdU proliferation index of epithelial cancer cells in AOM-induced tumors in $Tp53^{\Delta IEC}$;$Ikk\beta^{WT}$ (black bars) and $Tp53^{\Delta IEC}$;$Ikk\beta^{\Delta IEC}$ (gray bars) mice. Data are mean ± SE; n ≥ 5 tumors of each genotype.

(D) Number of cleaved caspase-3-positive epithelial cancer cells in AOM-induced tumors in $Tp53^{\Delta IEC}$;$Ikk\beta^{WT}$ (black bars) and $Tp53^{\Delta IEC}$;$Ikk\beta^{\Delta IEC}$ (gray bars) mice. Data are mean ± SE; n ≥ 5 tumors of each genotype.

(E and F) Incidence of invasive cancers in $Tp53^{\Delta IEC}$;$Ikk\beta^{WT}$ (black bars) and $Tp53^{\Delta IEC}$;$Ikk\beta^{\Delta IEC}$ (gray bars) mice. Data are mean ± SE; n = 9 animals/genotype; **p < 0.001 by t test.

(G–L) Immunohistochemical analysis of CXCL1 (G and H), F4/80 (I and J), and Gr-1 (K and L) in invasive cancers in $Tp53^{\Delta IEC}$;$Ikk\beta^{WT}$ (G, I, and K) and $Tp53^{\Delta IEC}$;$Ikk\beta^{\Delta IEC}$ (H, J, and L) mice. Note that CXCL1 is still expressed in tumor-infiltrating leukocytes, whereas it is absent in IECs of $Tp53^{\Delta IEC}$;$Ikk\beta^{\Delta IEC}$ mice. Scale bars represent 50 μm.

(M) Immunoblot analysis for the indicated proteins in lysates from invasive cancers from $Tp53^{\Delta IEC}$;$Ikk\beta^{WT}$ and $Tp53^{\Delta IEC}$;$Ikk\beta^{\Delta IEC}$ mice 18 weeks after the first AOM administration.

cells are recruited to, myeloid-specific $Ikk\beta$ deficiency markedly decreased proliferation of IECs, elevated the number of apoptotic IECs, and consequently decreased the extent of invasion (Figures 7D–7F, 7H, and 7I). Moreover, whereas metastatic spread could be observed in 30% of $Tp53^{\Delta IEC}$ mice adoptively transferred with control $Ikk\beta^{F/F}$ bone marrow, not a single metastasis was found when bone marrow from $Ikk\beta^{\Delta mye}$ mice was transplanted (Figure 7G). Recruitment of F4/80[+] and Gr1^{+} cells to the invasion front was not affected (data not shown), indicating that downregulation of NF-κB-dependent proinflammatory cytokines that could act in a paracrine manner was responsible for differences in proliferation and survival of invading tumor epithelia. Indeed, expression of mRNA encoding various cytokines, chemokines, and matrix metalloproteases was markedly downregulated (Figures 7J and 7K). We previously demonstrated in a model of colitis-associated tumorigenesis that gp130-dependent STAT3 activation rather than NF-κB signaling controls proliferation of AOM-mutagenized IECs (Bollrath et al., 2009; Greten et al., 2004). Similarly, and in line with decreased levels of the gp130/STAT3-activating cytokine IL-11, we observed a marked downregulation of tyrosine-phosphorylated STAT3 in invading $Tp53^{\Delta IEC}$ tumor epithelia when transplanted with bone marrow from $Ikk\beta^{\Delta mye}$ mice, whereas phosphorylation of IκBα was only moderately affected (Figures 7L–7O). Indeed, in $Tp53^{\Delta IEC}$ mice, strong nuclear accumulation of phosphorylated Stat3 was detected along the invasion front compared to noninvasive AOM-induced adenomas in wild-type mice, and this was even more pronounced in metastatic cells (Figure S5), suggesting that paracrine NF-κB-dependent activation of Stat3 is involved in the proliferation, survival, and metastatic spread of p53-deficient tumor cells. Importantly, in colon cancer patients, the degree of invasion and the occurrence of lymphatic metastases correlate with activation of STAT3 (Kusaba et al., 2005). Collectively, our results strongly support a key causal role of epithelial and myeloid IKKβ/NF-κB activation in the generation of an inflammatory microenvironment and the occurrence of EMT triggered by p53 deficiency leading to colonic tumor invasion and lymph node metastasis.

## $Tp53^{\Delta IEC}$ Mice Comprise a Suitable Model for Preclinical Studies

Because AOM-initiated tumors develop in the distal colon, they can be easily monitored by a mini endoscopy system (Figures 8A and 8B) (Becker et al., 2006). Thus, we reasoned that $Tp53^{\Delta IEC}$ mice might represent an excellent model for longitudinal preclinical therapeutic and endoscopic studies, considering that AOM-induced tumors range from the early noninvasive stage to fully metastasized invasive cancer. Miniprobe-based confocal laser scanning microscopy (CLSM) in combination with the intravenous application of fluorescein allows the evaluation of blood vessel length and area in vivo (Waldner et al., 2011) and has been successfully applied in human patients for the detection of endoscopically invisible neoplasia in Barrett's esophagus as well as for the diagnosis of biliary neoplasia (Meining et al., 2008; Pohl et al., 2008). To examine whether we could apply this method to monitor potential changes in vascularization during the carcinogenic process in p53-deficient tumors, we performed miniprobe-based CLSM in AOM-treated $Tp53^{\Delta IEC}$ mice at early and late tumor stages. In agreement

with the induction of an angiogenic switch (Bergers and Benjamin, 2003), a significant increase of blood vessel length and blood vessel area from early- to late-stage carcinogenesis could be detected by CLSM (Figures 8C–8F). This increase was confirmed by immunohistochemical staining of VE-cadherin in $Tp53^{\Delta IEC}$ tumors at 10 and 18 weeks after the first AOM injection, representing an early noninvasive as well as a late invasive stage of carcinogenesis (Figure 8G). Accordingly, $Tp53$-deficient cancers were characterized by a marked development of hypoxia (Figures 8H–8J), one of the prerequisites for the induction of an angiogenic switch (Bergers and Benjamin, 2003). We then assessed whether miniprobe-based CLSM could be applied for monitoring antiangiogenic therapy. Indeed, CLSM detected a significant decrease in vessel length and area upon treatment with the antiangiogenic receptor tyrosine kinase inhibitor sunitinib (Figures 8L and 8M), providing further evidence for the suitability of $Tp53^{\Delta IEC}$ mice in preclinical studies.

## DISCUSSION

$TP53$ is one of the most frequently mutated genes in human cancers, and loss of p53 is a late event in colorectal carcinogenesis and is associated with invasive growth (Fearon and Vogelstein, 1990; Levine and Oren, 2009). Although p53 deficiency in IECs is not sufficient to initiate spontaneous intestinal tumor development, 100% of $Tp53^{\Delta IEC}$ mice develop invasive cancer once challenged with a carcinogen that activates the Wnt pathway. Importantly, our results imply a context-dependent function of p53 during the intestinal carcinogenic process. During the initiation phase of the AOM model, p53 controls IEC survival and DNA repair, in agreement with its established role in response to genotoxic stress (Meek, 2009). However, in late-stage human adenomas, suppression of apoptosis does not correlate with loss of p53 (Fazeli et al., 1997). Based on our findings, we suggest that p53 suppresses an inflammatory microenvironment associated with the activation of NF-κB, which facilitates induction of EMT, during the progression stage. We provide evidence that NF-κB activation is indirectly triggered by elevated levels of circulating plasma LPS, a consequence of impaired intestinal epithelial barrier function in response to carcinogen exposure. Although attenuated tight-junction integrity can also be observed in p53 wild-type tumors, loss of p53 function seems to aggravate it. Whereas in respect to human cancers, one has to carefully consider that p53 function is presumably lost initially in only a few cells—in contrast to our mice that lack p53 in the entire colonic epithelium—it is important to note that the transition from adenoma to invasive cancer is also associated with an increased barrier defect in human disease (Soler et al., 1999). The particular indirect interaction between p53 and NF-κB shown here may be unique to colorectal carcinogenesis and may explain contrasting results regarding p53 function in other malignancies such as murine lymphoma, where p53 function is dispensable for lymphomagenesis in response to irradiation-triggered acute DNA damage (Christophorou et al., 2006). However, our results underscore the relevance of intestinal microorganisms for colon cancer progression, a notion that has been emerging over the last years for several inflammatory and malignant diseases (Hill and Artis, 2010).
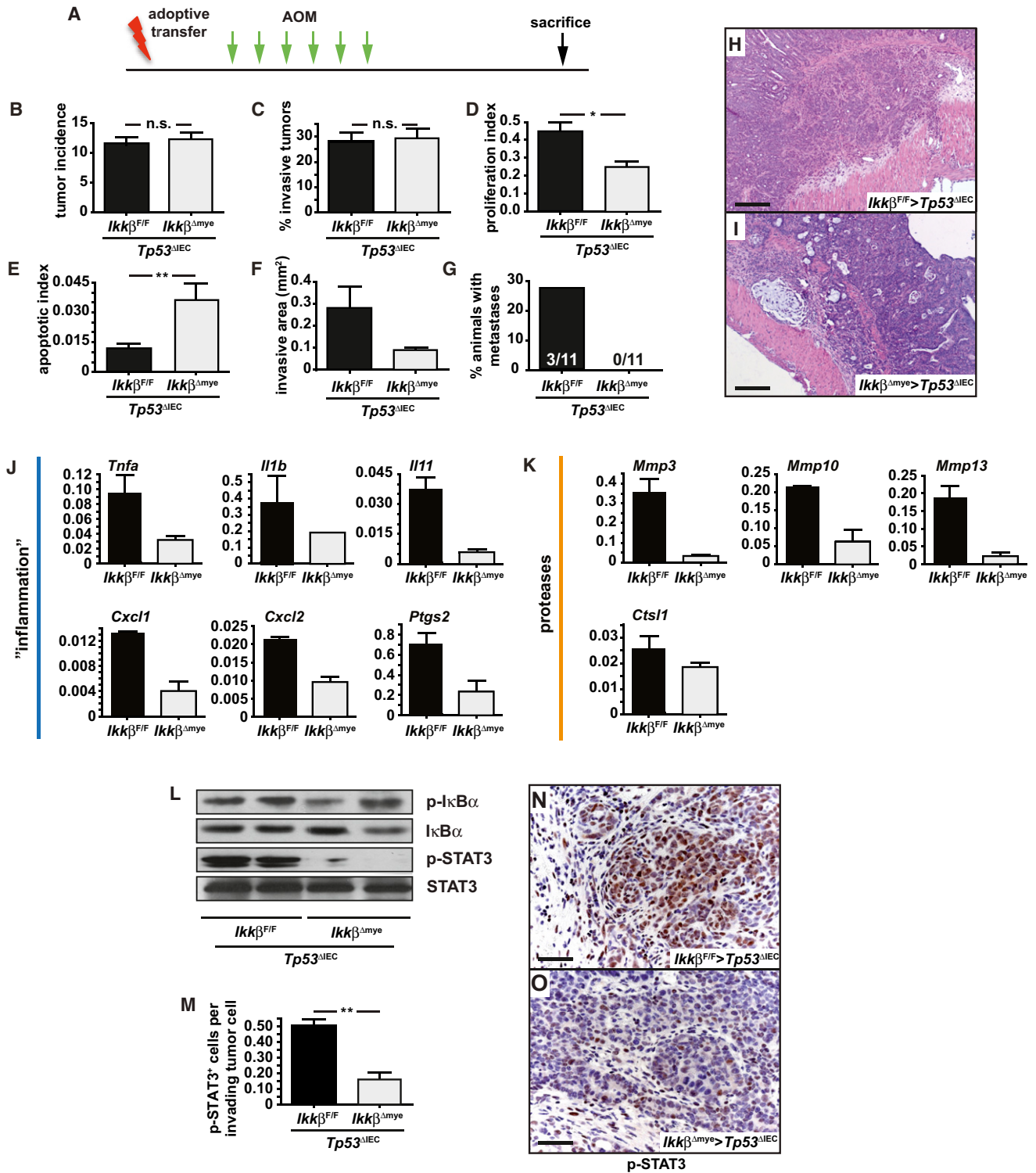
**Figure 7. Loss of *Ikkβ* in Myeloid Cells Suppresses Proliferation and Metastatic Spread of Invading Cancer Cells**

(A) Schematic representation of the model. $Tp53^{\Delta IEC}$ animals were lethally irradiated and transplanted with bone marrow from $Ikk\beta^{F/F}$ or $Ikk\beta^{\Delta mye}$ mice. Eight weeks later, AOM was injected once weekly for six weeks. Mice were analyzed 10–13 weeks after the first AOM administration.

(B) Tumor incidence in AOM-injected $Tp53^{\Delta IEC}$ mice transplanted with bone marrow from $Ikk\beta^{F/F}$ (black bars) or $Ikk\beta^{\Delta mye}$ (gray bars) mice. Data are mean ± SE; n = 11 animals/genotype. n.s., not significant.

(C) Incidence of invasive cancers in AOM-injected $Tp53^{\Delta IEC}$ mice transplanted with bone marrow from $Ikk\beta^{F/F}$ (black bars) or $Ikk\beta^{\Delta mye}$ (gray bars) mice. Data are mean ± SE; n = 11 animals/genotype.

*(legend continued on next page)*

Our findings demonstrate that IKKβ/NF-κB can have distinct functions during different phases of colonic tumor development. During colitis-associated tumorigenesis in p53-proficient mice, NF-κB is mainly responsible for transcriptional upregulation of antiapoptotic genes during the promotion stage. However, in the absence of p53, NF-κB activation induces Twist expression, thereby allowing EMT induction, which presumably is a prerequisite for the invasion of AOM-mutagenized colonocytes. Furthermore, recruitment of myeloid cells and their release of NF-κB-dependent proinflammatory cytokines enforce a feedforward loop and activate STAT3 in invading cancer cells to stimulate their proliferation, survival, and metastatic spread.

Our data contrast with previous findings in $Apc^{Min/+}$ mice, where p53 deficiency did not affect tumor incidence or progression (Clarke et al., 1995; Fazeli et al., 1997). One possible explanation might be that other malignancies developed in the complete absence of p53, which may have affected intestinal tumor progression or shortened the life span of the mice. Another possibility is that mice on mixed genetic backgrounds were used in those previous studies. Accordingly, when mice on a pure genetic background were studied, p53-deficient $Apc^{Min/+}$ mice showed a tendency toward enhanced tumor progression and the development of invasive cancer (Halberg et al., 2000). Recently, it was suggested that p53 controls a specific gene signature to suppress intestinal tumor progression in a $Csnk1a1$-deficient background (Elyada et al., 2011). However, we did not detect enrichment of these genes in AOM-initiated cancers (data not shown). Presumably, tumor location (small intestine versus colon) and/or mode of Wnt activation ($Csnk1a1$ ablation versus stabilizing $Ctnnb1$ mutations) account for this difference. Only very few mouse models of intestinal tumorigenesis develop invasive colon cancer and metastasize. To date, it remains unclear which pathways are essential specifically for colonic tumor progression in mice. Concomitant activation of oncogenic K-ras and conditional loss of $Apc$ led to submucosal invasion and liver metastases in about 20% of these mice (Hung et al., 2010). However, AOM-induced carcinomas in $Tp53^{\Delta IEC}$ mice did not harbor any $K$-ras mutations (data not shown). Furthermore, oncogenic K-ras activation in IECs does not promote invasion in the AOM model (Bennecke et al., 2010). Our data strongly support that loss of p53 and the associated NF-κB activation culminating in EMT could be among the essential events that regulate colonic tumor progression.

Interestingly, AOM-challenged $Tp53^{\Delta IEC}$ mice developed only lymph node metastases. Here, we provide evidence that NF-κB activation in colon tumors is also associated with the presence of lymph node metastasis in human patients. Similarly, overexpression of the two well-described NF-κB target gene products CXCL1 and Twist correlates with nodal invasion in colon cancer patients (Ogata et al., 2010; Valdés-Mora et al., 2009), further underlining the relevance of $Tp53^{\Delta IEC}$ mice for human disease.

One goal of generating an autochthonous immune-competent mouse model that faithfully recapitulates the histopathology and genetic alterations of specific human cancer is to functionally investigate the biological basis of tumor development. Another important aim of such an effort is to create an animal model that can be used in translational preclinical studies. Our model presented here achieves both aims. Morphological appearance of p53-deficient tumors and their gene signature reveals high resemblance to invasive human colon cancer. Thus, AOM-initiated $Tp53^{\Delta IEC}$ mice comprise a well-suited model to dissect the importance of the different inflammatory signaling pathways in the various cellular compartments of the tumor microenvironment to further understand the molecular mechanisms leading to metastasis. Furthermore, tumor location and the possibility of endoscopic monitoring make this model suitable for translational diagnostic and therapeutic studies.

## EXPERIMENTAL PROCEDURES

### Mice

To delete exons 2–10 of $Tp53$ in IECs, we crossed floxed $Tp53$ (Jonkers et al., 2001) obtained from the National Cancer Institute to $villin$-Cre (Madison et al., 2002) or $villin$-CreER$^{T2}$ (el Marjou et al., 2004) mice. $Ikk\beta^{F/F}$ and $Ikk\beta^{\Delta mye}$ have been described previously (Greten et al., 2004). All mice including littermate controls were crossed on an FVB background for at least four generations, and in all experiments littermate controls were used. In $villin$-CreER$^{T2}$ mice, deletion was induced by five daily oral administrations of 1 mg tamoxifen (Sigma) in an ethanol/oil mixture. In adoptive transfer experiments, $Tp53^{\Delta IEC}$ mice were irradiated (9 Gy) and $2 \times 10^6$ bone marrow cells from $Ikk\beta^{F/F}$ or $Ikk\beta^{\Delta mye}$ mice were transferred by tail vein injection. Eight weeks after transplantation, AOM injections commenced. Azoxymethane (Sigma) was injected intraperitoneally (i.p.) once a week for 6 weeks at 10 mg/kg. Sunitinib (40 mg/kg) was applied daily by oral gavage for 14 days. Mini endoscopy was performed on anesthetized mice using a mouse mini endoscopy system (Karl Storz). A confocal miniprobe (Mauna Kea Technologies) was applied via the working channel of the endoscope, and video sequences (each 20 s, 12 frames/s) were recorded within 10 min after intravenous injection of 100 μl fluorescein (1%). Vessel length and area of a minimum of ten images per

(D and E) Index of BrdU-positive cells (D) and cleaved caspase-3-positive cells (E) along the invasion front of cancers in AOM-injected $Tp53^{\Delta IEC}$ mice transplanted with bone marrow from $Ikk\beta^{F/F}$ (black bars) or $Ikk\beta^{\Delta mye}$ (gray bars) mice. Data are mean ± SE; n ≥ 5 animals/genotype; **p < 0.001 by t test.

(F) Total invasive area/animal in cancers in AOM-injected $Tp53^{\Delta IEC}$ mice transplanted with bone marrow from $Ikk\beta^{F/F}$ (black bars) or $Ikk\beta^{\Delta mye}$ (gray bars) mice. Data are mean ± SE; n = 11 animals/genotype.

(G) Incidence of invasive cancers in AOM-injected $Tp53^{\Delta IEC}$ mice transplanted with bone marrow from $Ikk\beta^{F/F}$ (black bars) or $Ikk\beta^{\Delta mye}$ (gray bars) mice.

(H and I) Representative H&E-stained sections of colons from AOM-injected $Tp53^{\Delta IEC}$ mice transplanted with bone marrow from $Ikk\beta^{F/F}$ (Ikkβ$^{F/F}$>Tp53$^{\Delta IEC}$) or $Ikk\beta^{\Delta mye}$ (Ikkβ$^{\Delta mye}$>Tp53$^{\Delta IEC}$) mice. Scale bars represent 200 μm.

(J and K) Relative expression levels of mRNAs isolated from AOM-induced tumor tissues of $Tp53^{\Delta IEC}$ mice transplanted with bone marrow from $Ikk\beta^{F/F}$ (black bars) or $Ikk\beta^{\Delta mye}$ (gray bars) mice and analyzed by real-time PCR. Data are mean ± SE; n = 2/genotype.

(L) Immunoblot analysis for the indicated proteins in lysates from invasive cancers from $Tp53^{\Delta IEC}$ mice transplanted with bone marrow from $Ikk\beta^{F/F}$ or $Ikk\beta^{\Delta mye}$ mice.

(M) Average number of p-STAT3-positive cells/invading tumor epithelial cells in AOM-injected $Tp53^{\Delta IEC}$ mice transplanted with bone marrow from $Ikk\beta^{F/F}$ (black bars) or $Ikk\beta^{\Delta mye}$ (gray bars) mice. Data are mean ± SE; n ≥ 4 animals/genotype; **p < 0.001 by t test.

(N and O) Immunohistochemical analysis of p-STAT3 in invasive cancers of AOM-challenged $Tp53^{\Delta IEC}$ mice transplanted with bone marrow from $Ikk\beta^{F/F}$ (N) or $Ikk\beta^{\Delta mye}$ (O) mice. Scale bars represent 50 μm.
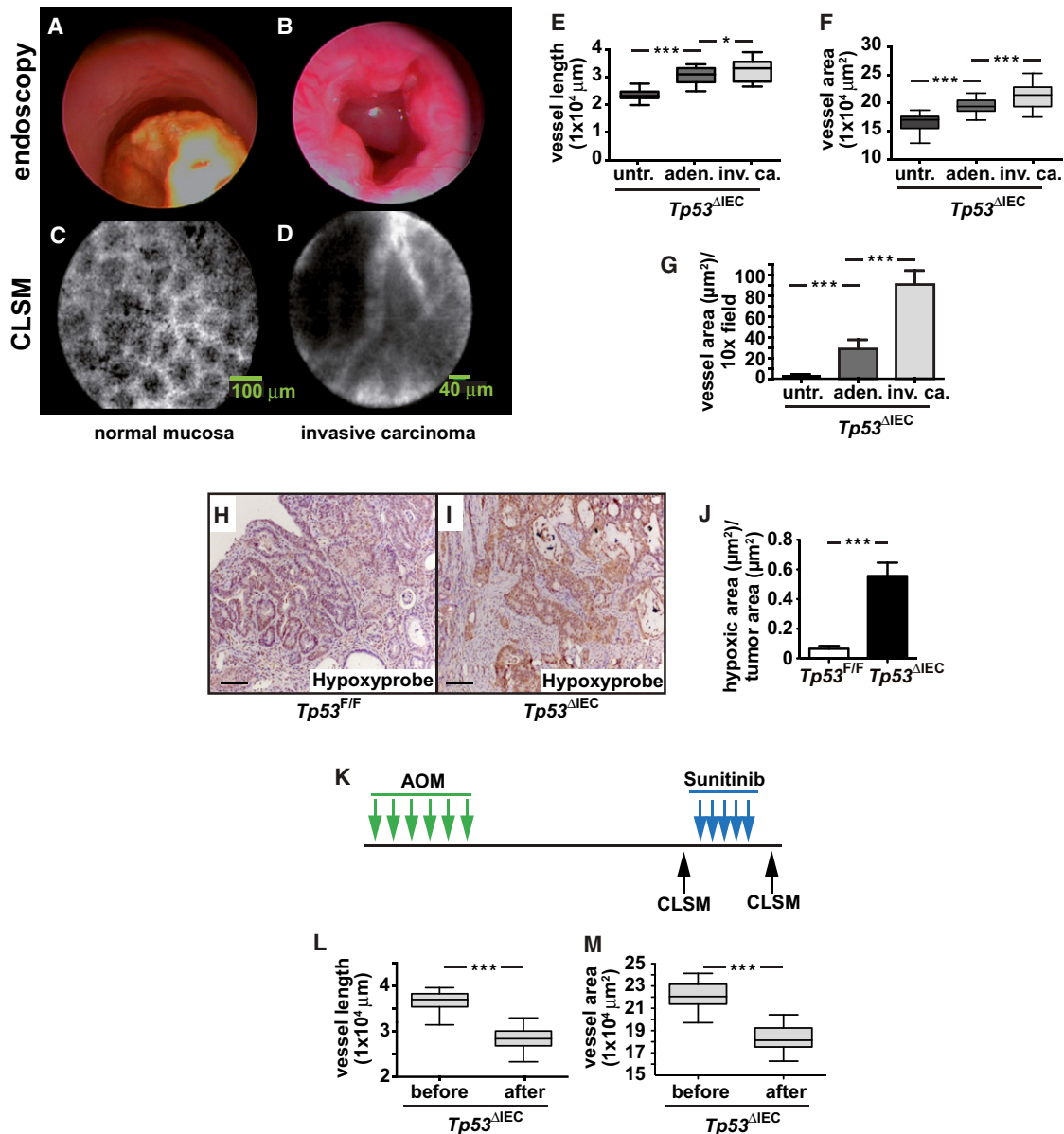
See also Figure S5.

**Figure 8. Increased Vascularization in p53-Deficient Carcinomas Can Be Evaluated by Endoscopically Guided Confocal Laser Scanning Microscopy**

(A–D) Representative images obtained by white-light mini endoscopy (A and B) and confocal laser scanning microscopy of fluorescein-injected animals (C and D) in unchallenged (A and C) and AOM-initiated $Tp53^{\Delta IEC}$ mice with invasive cancer (B and D).

(E and F) Quantification of blood vessel length (E) and blood vessel area (F) in untreated animals (untr.) and noninvasive (aden.) and invasive cancers (inv. ca.) in $Tp53^{\Delta IEC}$ mice by CLSM. Data are mean ± SE; n ≥ 4. *p < 0.05, ***p < 0.0001 by t test.

(G) Quantification of blood vessel area in untreated animals and noninvasive and invasive cancers in $Tp53^{\Delta IEC}$ mice. Vessels were visualized by immunohisto-chemical staining for VE-cadherin, and the area was measured per 100× magnification field on a Zeiss Axio Imager using AxioVision software. Data are mean ± SE; n ≥ 6; ***p < 0.0001 by t test.

(H and I) Immunohistochemical analysis of tissue hypoxia using Hypoxyprobe, demonstrating increased levels of hypoxia in invasive cancers from $Tp53^{\Delta IEC}$ mice (I) compared to noninvasive adenomas from $Tp53^{F/F}$ mice (H) 16 weeks after the first AOM administration. Scale bars represent 100 μm.

(J) Quantification of hypoxic areas normalized to tumor area in noninvasive adenomas from $Tp53^{F/F}$ mice and invasive cancers from $Tp53^{\Delta IEC}$ mice 16 weeks after the first AOM administration. Data are mean ± SE; n ≥ 4; ***p < 0.0001 by t test.

(K) Schematic representation of the order of AOM and sunitinib administration and when CLSM was performed.

(L and M) Quantification of blood vessel length (L) and blood vessel area (M) by CLSM in established tumors in fluorescein-injected $Tp53^{\Delta IEC}$ mice before and after sunitinib treatment. Data are mean ± SE; n ≥ 4; ***p < 0.0001 by t test.

tumor were quantified using Cellvizio software. To measure intestinal barrier permeability, noncharged FITC-dextran (MW 4000; Sigma) was prepared at 80 mg/ml in PBS. Mice were orally gavaged with 60 mg per 100 g of body weight. After 4 hr, serum was collected and FITC-dextran was measured using a fluorometer (BMG Labtech FLUOstar Orange) at 485 nm excitation and 510 nm emission. Bacterial endotoxin levels were determined using an endpoint chromogenic Limulus Amebocyte Lysate assay (Lonza) according to the manufacturer's instructions. To deplete intestinal microflora, mice were treated with a combination of ampicillin (0.22 g/l), vancomycin (0.1 g/l), neomycin (0.214 g/l), and metronidazole (0.213 g/l) for 2 weeks. All procedures were reviewed and approved by the Regierung von Oberbayern.

### Human Samples

Human tumor samples were collected within the first 30 min after resection. Tumors were macroscopically dissected by an experienced pathologist, snap-frozen, and stored in liquid nitrogen ($-196^{\circ}C$) until usage. Before molecular analysis, tumor diagnosis was confirmed and tumor content (at least 70%) was determined by hematoxylin-eosin staining. All procedures were performed with the approval of the ethics committee of the Technical University of Munich on samples from subjects who had given their written informed consent.

### Protein Analysis

Isolation of IECs and immunoblot analysis were performed as previously described (Bollrath et al., 2009). The following antibodies were used in immunoblot analysis: β-actin (Sigma; A4700), IκBα (Santa Cruz; sc-371), phospho-IκBα (Cell Signaling; 9241), p65 (Santa Cruz; SC-372), phospho-p65 (Cell Signaling; 3037), E-cadherin (Becton Dickinson; 610182), and Twist (Abcam; 49254). NF-κB binding activity was determined using an Odyssey infrared EMSA kit (LICOR). Ten micrograms of protein sample was incubated with 1 μM 3′ DY682-labeled NF-κB consensus oligo. Samples were run on a 5% native TBE acrylamide gel, and bands were detected on an Odyssey infrared imaging system.

### Histological Analysis

Standard immunohistochemical procedures were performed using the following antibodies: β-catenin (Santa Cruz; sc-1496), bromodeoxyuridine (BrdU) (AbD Serotec; MCA 2060), cleaved caspase-3 (Cell Signaling; 9661), CXCL1 (R&D Systems; MAB453), F4/80 (Caltag; MF48000), Gr-1 (eBioscience; 12-5931-82), phospho-Histone H2A.X (Cell Signaling; 2577), E-cadherin (Becton Dickinson; 610182), Twist (Abcam; 49254), vimentin (Santa Cruz; SC-7557), VE-cadherin (Santa Cruz; SC-6458), and occludin (Invitrogen; 711500). For immunofluorescent detection of E-cadherin, the Vector Labs Mouse on Mouse kit was used; vimentin and occludin were detected using Alexa Fluor 594-labeled anti-goat antibody (Invitrogen). Alcian blue staining was performed to detect acetic mucins and mucosubstances according to standard procedures. Paneth cells were detected by azure-eosin staining. For detection of apoptosis, the ApoAlert DNA Fragmentation Assay kit (Clontech; 630108) was used according to the manufacturer's instructions. For the detection of tissue hypoxia, the Hypoxyprobe-1 Plus kit (Chemicon International; HP2-100) was used according to the manufacturer's instructions. In brief, 60 mg/kg body weight of pimonidazole hydrochloride was injected i.p. 1 hr before sacrifice. In hypoxic tissues, reductively activated 2-nitroimidazole protein adducts were detected by the peroxidase immunohistochemistry technique using FITC-conjugated mAb directed against pimonidazole protein adducts and a secondary mouse anti-FITC mAb conjugated to HRP. Hematoxylin was used for counterstaining.

### Statistical Analysis

Data are expressed as mean ± SEM. Differences were analyzed by Student's t test using Prism5 (GraphPad Software). The p values $\leq 0.05$ were considered significant.

### ACCESSION NUMBERS

Gene expression and array comparative genomic hybridization raw data have been deposited in the Gene Expression Omnibus database under accession numbers GSE27868 and GSE28129, respectively.

### SUPPLEMENTAL INFORMATION

Supplemental Information includes five figures and Supplemental Experimental Procedures and can be found with this article online at http://dx.doi.org/10.1016/j.ccr.2012.11.014.

### REFERENCES

Becker, C., Fantini, M.C., and Neurath, M.F. (2006). High resolution colonoscopy in live mice. Nat. Protoc. *1*, 2900–2904.

Bennecke, M., Kriegl, L., Bajbouj, M., Retzlaff, K., Robine, S., Jung, A., Arkan, M.C., Kirchner, T., and Greten, F.R. (2010). Ink4a/Arf and oncogene-induced senescence prevent tumor progression during alternative colorectal tumorigenesis. Cancer Cell *18*, 135–146.

Bergers, G., and Benjamin, L.E. (2003). Tumorigenesis and the angiogenic switch. Nat. Rev. Cancer *3*, 401–410.

Bollrath, J., and Greten, F.R. (2009). IKK/NF-κB and STAT3 pathways: central signalling hubs in inflammation-mediated tumour promotion and metastasis. EMBO Rep. *10*, 1314–1319.

Bollrath, J., Phesse, T.J., von Burstin, V.A., Putoczki, T., Bennecke, M., Bateman, T., Nebelsiek, T., Lundgren-May, T., Canli, O., Schwitalla, S., et al. (2009). gp130-mediated Stat3 activation in enterocytes regulates cell survival and cell-cycle progression during colitis-associated tumorigenesis. Cancer Cell *15*, 91–102.

Christophorou, M.A., Ringshausen, I., Finch, A.J., Swigart, L.B., and Evan, G.I. (2006). The pathological response to DNA damage does not contribute to p53-mediated tumour suppression. Nature *443*, 214–217.

Clarke, A.R., Cummings, M.C., and Harrison, D.J. (1995). Interaction between murine germline mutations in p53 and APC predisposes to pancreatic neoplasia but not to increased intestinal malignancy. Oncogene *11*, 1913–1920.

Egan, L.J., Eckmann, L., Greten, F.R., Chae, S., Li, Z.W., Myhre, G.M., Robine, S., Karin, M., and Kagnoff, M.F. (2004). IκB-kinaseβ-dependent NF-κB activation provides radioprotection to the intestinal epithelium. Proc. Natl. Acad. Sci. USA *101*, 2452–2457.

el Marjou, F., Janssen, K.P., Chang, B.H., Li, M., Hindie, V., Chan, L., Louvard, D., Chambon, P., Metzger, D., and Robine, S. (2004). Tissue-specific and inducible Cre-mediated recombination in the gut epithelium. Genesis *39*, 186–193.

Elyada, E., Pribluda, A., Goldstein, R.E., Morgenstern, Y., Brachya, G., Cojocaru, G., Snir-Alkalay, I., Burstain, I., Haffner-Krausz, R., Jung, S., et al. (2011). CKIα ablation highlights a critical role for p53 in invasiveness control. Nature *470*, 409–413.

Fazeli, A., Steen, R.G., Dickinson, S.L., Bautista, D., Dietrich, W.F., Bronson, R.T., Bresalier, R.S., Lander, E.S., Costa, J., and Weinberg, R.A. (1997). Effects of p53 mutations on apoptosis in mouse intestinal and human colonic adenomas. Proc. Natl. Acad. Sci. USA *94*, 10199–10204.

Fearon, E.R., and Vogelstein, B. (1990). A genetic model for colorectal tumorigenesis. Cell *61*, 759–767.

Fodde, R., Smits, R., and Clevers, H. (2001). APC, signal transduction and genetic instability in colorectal cancer. Nat. Rev. Cancer 1, 55–67.

Greten, F.R., Eckmann, L., Greten, T.F., Park, J.M., Li, Z.W., Egan, L.J., Kagnoff, M.F., and Karin, M. (2004). IKKβ links inflammation and tumorigenesis in a mouse model of colitis-associated cancer. Cell 118, 285–296.

Grivennikov, S.I., Greten, F.R., and Karin, M. (2010). Immunity, inflammation, and cancer. Cell 140, 883–899.

Hahn, W.C., and Weinberg, R.A. (2002). Rules for making human tumor cells. N. Engl. J. Med. 347, 1593–1603.

Halberg, R.B., Katzung, D.S., Hoff, P.D., Moser, A.R., Cole, C.E., Lubet, R.A., Donehower, L.A., Jacoby, R.F., and Dove, W.F. (2000). Tumorigenesis in the multiple intestinal neoplasia mouse: redundancy of negative regulators and specificity of modifiers. Proc. Natl. Acad. Sci. USA 97, 3461–3466.

Hanahan, D., and Weinberg, R.A. (2011). Hallmarks of cancer: the next generation. Cell 144, 646–674.

Hill, D.A., and Artis, D. (2010). Intestinal bacteria and the regulation of immune cell homeostasis. Annu. Rev. Immunol. 28, 623–667.

Horst, D., Budczies, J., Brabletz, T., Kirchner, T., and Hlubek, F. (2009). Invasion associated up-regulation of nuclear factor κB target genes in colorectal cancer. Cancer 115, 4946–4958.

Hung, K.E., Maricevich, M.A., Richard, L.G., Chen, W.Y., Richardson, M.P., Kunin, A., Bronson, R.T., Mahmood, U., and Kucherlapati, R. (2010). Development of a mouse model for sporadic and metastatic colon tumors and its use in assessing drug treatment. Proc. Natl. Acad. Sci. USA 107, 1565–1570.

Jang, K.T., Chae, S.W., Sohn, J.H., Park, H.R., and Shin, H.S. (2002). Coexpression of MUC1 with p53 or MUC2 correlates with lymph node metastasis in colorectal carcinomas. J. Korean Med. Sci. 17, 29–33.

Jonkers, J., Meuwissen, R., van der Gulden, H., Peterse, H., van der Valk, M., and Berns, A. (2001). Synergistic tumor suppressor activity of BRCA2 and p53 in a conditional mouse model for breast cancer. Nat. Genet. 29, 418–425.

Joyce, J.A., and Pollard, J.W. (2009). Microenvironmental regulation of metastasis. Nat. Rev. Cancer 9, 239–252.

Kawauchi, K., Araki, K., Tobiume, K., and Tanaka, N. (2008). p53 regulates glucose metabolism through an IKK-NF-κB pathway and inhibits cell transformation. Nat. Cell Biol. 10, 611–618.

Kusaba, T., Nakayama, T., Yamazumi, K., Yakata, Y., Yoshizaki, A., Nagayasu, T., and Sekine, I. (2005). Expression of p-STAT3 in human colorectal adenocarcinoma and adenoma; correlation with clinicopathological factors. J. Clin. Pathol. 58, 833–838.

Levine, A.J., and Oren, M. (2009). The first 30 years of p53: growing ever more complex. Nat. Rev. Cancer 9, 749–758.

Madison, B.B., Dunbar, L., Qiao, X.T., Braunstein, K., Braunstein, E., and Gumucio, D.L. (2002). cis elements of the villin gene control expression in restricted domains of the vertical (crypt) and horizontal (duodenum, cecum) axes of the intestine. J. Biol. Chem. 277, 33275–33283.

Mantovani, A., Allavena, P., Sica, A., and Balkwill, F. (2008). Cancer-related inflammation. Nature 454, 436–444.

Meek, D.W. (2009). Tumour suppression by p53: a role for the DNA damage response? Nat. Rev. Cancer 9, 714–723.

Meining, A., Frimberger, E., Becker, V., Von Delius, S., Von Weyhern, C.H., Schmid, R.M., and Prinz, C. (2008). Detection of cholangiocarcinoma in vivo using miniprobe-based confocal fluorescence microscopy. Clin. Gastroenterol. Hepatol. 6, 1057–1060.

Murdoch, C., Muthana, M., Coffelt, S.B., and Lewis, C.E. (2008). The role of myeloid cells in the promotion of tumour angiogenesis. Nat. Rev. Cancer 8, 618–631.

Ogata, H., Sekikawa, A., Yamagishi, H., Ichikawa, K., Tomita, S., Imura, J., Ito, Y., Fujita, M., Tsubaki, M., Kato, H., et al. (2010). GROα promotes invasion of colorectal cancer cells. Oncol. Rep. 24, 1479–1486.

Pohl, H., Rösch, T., Vieth, M., Koch, M., Becker, V., Anders, M., Khalifa, A.C., and Meining, A. (2008). Miniprobe confocal laser microscopy for the detection of invisible neoplasia in patients with Barrett's oesophagus. Gut 57, 1648–1653.

Polyak, K., and Weinberg, R.A. (2009). Transitions between epithelial and mesenchymal states: acquisition of malignant and stem cell traits. Nat. Rev. Cancer 9, 265–273.

Qiu, W., Carson-Walter, E.B., Kuan, S.F., Zhang, L., and Yu, J. (2009). PUMA suppresses intestinal tumorigenesis in mice. Cancer Res. 69, 4999–5006.

Riley, T., Sontag, E., Chen, P., and Levine, A. (2008). Transcriptional control of human p53-regulated genes. Nat. Rev. Mol. Cell Biol. 9, 402–412.

Soler, A.P., Miller, R.D., Laughlin, K.V., Carp, N.Z., Klurfeld, D.M., and Mullin, J.M. (1999). Increased tight junctional permeability is associated with the development of colon cancer. Carcinogenesis 20, 1425–1431.

Toft, N.J., Winton, D.J., Kelly, J., Howard, L.A., Dekker, M., te Riele, H., Arends, M.J., Wyllie, A.H., Margison, G.P., and Clarke, A.R. (1999). Msh2 status modulates both apoptosis and mutation frequency in the murine small intestine. Proc. Natl. Acad. Sci. USA 96, 3911–3915.

Valdés-Mora, F., Gómez del Pulgar, T., Bandrés, E., Cejas, P., Ramírez de Molina, A., Pérez-Palacios, R., Gallego-Ortega, D., García-Cabezas, M.A., Casado, E., Larrauri, J., et al. (2009). TWIST1 overexpression is associated with nodal invasion and male sex in primary colorectal cancer. Ann. Surg. Oncol. 16, 78–87.

Vogelstein, B., Fearon, E.R., Hamilton, S.R., Kern, S.E., Preisinger, A.C., Leppert, M., Nakamura, Y., White, R., Smits, A.M., and Bos, J.L. (1988). Genetic alterations during colorectal-tumor development. N. Engl. J. Med. 319, 525–532.

Waldner, M.J., Wirtz, S., Neufert, C., Becker, C., and Neurath, M.F. (2011). Confocal laser endomicroscopy and narrow-band imaging-aided endoscopy for in vivo imaging of colitis and colon cancer in mice. Nat. Protoc. 6, 1471–1481.

Wang, X., Tully, O., Ngo, B., Zitin, M., and Mullin, J.M. (2011). Epithelial tight junctional changes in colorectal cancer tissues. ScientificWorldJournal 11, 826–841.

Webster, G.A., and Perkins, N.D. (1999). Transcriptional cross talk between NF-κB and p53. Mol. Cell. Biol. 19, 3485–3495.

Wood, L.D., Parsons, D.W., Jones, S., Lin, J., Sjöblom, T., Leary, R.J., Shen, D., Boca, S.M., Barber, T., Ptak, J., et al. (2007). The genomic landscapes of human breast and colorectal cancers. Science 318, 1108–1113.